Journal of Power Sources 189 (2009) 1154–1163

Contents lists available at ScienceDirect

Journal of Power Sources

journal homepage: www.elsevier.com/locate/jpowsour

Structural and magnetic properties of $Li_x(Mn_yFe_{1-y})PO_4$ electrode materials for Li-ion batteries

M. Kopec[a], A. Yamada[b], G. Kobayashi[b], S. Nishimura[b], R. Kanno[b], A. Mauger[c,*], F. Gendron[a], C.M. Julien[a]

[a] Université Paris-6, UMR 7588, Institut des Nanosciences de Paris, 140 rue de Lourmel, 75015 Paris, France
[b] Department of Electronic Chemistry, Interdisciplinary Graduate School of Science and Engineering, Tokyo Institute of Technology, 4259 Nagatsuta, Midori, 226-8502 Yokohama, Japan
[c] Université Paris-6, UMR7590, Institut de Minéralogie et Physique de la Matière Condensée, 140 rue de Lourmel, 75015 Paris, France

ARTICLE INFO

Article history:
Received 27 November 2008
Accepted 21 December 2008
Available online 30 December 2008

Keywords:
Olivine
Insertion compounds
Li-ion batteries

ABSTRACT

A series of $LiMn_yFe_{1-y}PO_4$ samples have been prepared in the whole range $0 \le y \le 1$. Chemical delithiation could be achieved to obtain $Mn_yFe_{1-y}PO_4$ in the range $0 \le y \le 0.8$, keeping the same crystal phase (olivine structure, space group *Pnma*). The composition $y = 0.8$ is the limit where the delithiated phase is still crystallized, but abruptly suffers strains at the molecular scale evidenced by both optical spectroscopy and X-ray diffraction. The analysis of the magnetic properties shows that in all the samples the concentration of impurities is negligible. The concentration of polarons, either holes associated to Li vacancies in $LiMn_yFe_{1-y}PO_4$ or electrons associated to the existence of Li left in the matrix of $Mn_yFe_{1-y}PO_4$, is found to be small (≤1%) in all the samples. For $y \le 0.6$, all the Mn^{3+} ions $Mn_yFe_{1-y}PO_4$ are in the high-spin state ($S = 2$). At larger manganese concentration, however, the Mn^{3+} ions in excess of the critical concentration $y_c = 0.6$ undergo a transition to the low-spin state ($S = 1$). As a consequence, and in contrast with prior works, we find that $Mn_{0.8}Fe_{0.2}PO_4$ has magnetic interactions that are much smaller, and no antiferromagnetic ordering in this compound is detected, at least above 20 K. Antiferromagnetic ordering that had been reported so far for $Mn_yFe_{1-y}PO_4$ at large y-composition might come from incomplete delithiation. The spin-transition of Mn^{3+} in concentration $(y-y_c)$ to the low-spin state is at the origin of the strain fields at the molecular scale that increase with y for $y > 0.6$, and ultimately prevents the full delithiation for $y > 0.8$. This result sheds light on the reason for the degradation of cathode properties in Mn-rich compounds of the heterosite–purpurite series, while the electrochemical properties are good in the range $y \le 0.6$ but only at slow rates, due to the very small hopping mobility of the small polaron.

© 2008 Elsevier B.V. All rights reserved.

1. Introduction

The lithium orthophosphates $LiMPO_4$ (M = Fe, Mn, Co, Ni) crystallize in the olivine *Pnma* structure illustrated in Fig. 1. It can be viewed as layers formed by corner-sharing MO_6 octahedra. These layers are linked by PO_4 tetrahedra to form a distorted hexagonal structure, leaving space for channels of lithium ions along the *b*-axis. Such a structure gives these compounds a potential for their use as the active cathode element of rechargeable lithium batteries that has been recognized 10 years ago [1]. Since then, much attention has been focused on $LiFePO_4$, because of its low cost, non-toxicity, and an outstanding thermal stability. However, $LiMnPO_4$ has in principle some advantages over its Fe-partner. The theoretical energy density of $LiMnPO_4$ is 697 Wh kg^{-1}, against 586 Wh kg^{-1} for $LiFePO_4$. The Mn^{3+}/Mn^{2+} redox couple is 4.1 V vs. Li^0/Li^+ against 3.5 V for the Fe^{3+}/Fe^{2+} couple, and 4.1 V is still small enough to avoid any decomposition of the organic electrolyte. However, the electrochemical properties of $LiMnPO_4$ have been a disappointment. Despite the higher open-circuit voltage, the current density allowed for electrode operation of Li_xMnPO_4 is several orders of magnitude smaller than that of Li_xFePO_4 [2,3], and the kinetics are much slower [1,4,5].

Several reasons have been invoked to explain the low electrochemical activity of the Mn^{3+}/Mn^{2+} redox couple. One is the localization of small polaronic holes on Mn^{3+} sites [5]. This hypothesis has been sustained by transport experiments that have shown a much higher activation energy E_a of the electronic conductivity, E_a raising to 1 eV in $LiMnPO_4$ [6], against 0.6 eV in $LiFePO_4$ [6,7]. Since this activation energy is the energy barrier that a small polaron has to overcome to hop on a neighboring site, the higher value of E_a means a stronger localization on Mn^{3+} than on Fe^{3+}, and results in

* Corresponding author. Tel.: +33 144274439; fax: +33 144273882.
E-mail address: alain.mauger@impmc.jussieu.fr (A. Mauger).

0378-7753/$ – see front matter © 2008 Elsevier B.V. All rights reserved.
doi:10.1016/j.jpowsour.2008.12.096

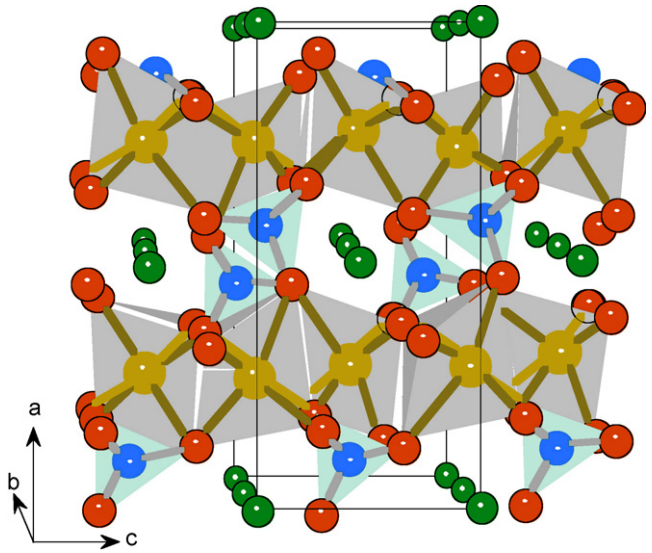

Fig. 1. Structure of the olivine-like $LiMn_yFe_{1-y}PO_4$ compounds. The $Fe(Mn)O_6$ octahedra are dashed with grey color for clarity and form layers in the *bc* plane. Adjacent layers are linked by PO_4 units, leaving some place for one-dimensional arrays of Li atoms along the *a*-axis (P is in blue, oxygen in red and Li in green). (For interpretation of the references to color in this figure legend, the reader is referred to the web version of the article.)

a lowering of the electronic conductivity by more than five orders of magnitude as compared to $LiFePO_4$ [6].

In this context, the investigation of the $LiMn_yFe_{1-y}PO_4$ series is of interest, because an intermediate composition y may realize a compromise to avoid these drawbacks at $y = 1$, and yet win some efficiency expected from the higher open-circuit voltage by substituting some of the Fe ions by Mn ions. Such investigations have been performed in the recent past [8], which confirmed that the maximum capacity at the 4.1 V plateau for the Mn^{3+}/Mn^{2+} composition is obtained at the medium composition $y \approx 0.5$ (the theoretical capacity is obtained in this case).

A key aspect of this material that impairs the electrochemical performance is the significant loss of long-range order and strong deformations upon delithiation [3–5]. These deformations have been linked to the fact that Mn^{3+} is a Jahn-Teller ion that induces lattice distortions. Indeed, the analysis of the X-ray diffraction (XRD) spectra of $LiMn_yFe_{1-y}PO_4$ in the present work reveals a decrease of the lattice coherence length upon delithiation in the whole range of manganese concentration for $y \leq 0.6$. It means that the local distortion by JT effect and the large volume mismatch as well (ca. 12% between $LiMnPO_4$ and $MnPO_4$) induce dislocations and cracks at the two-phase interface region during lithiation/delithiation processes. We shall see in this work, with spectroscopic and magnetic approaches, that the critical composition for dramatic effects on such crystal coherence effects is $y = 0.8$, which is consistent with the previous reports based on XRD [4,5]. Such extended defects may disturb the facile electrode reactions [9]. However, the Jahn-Teller effect itself cannot prevent the natural crystallization of $MnPO_4$ in the olivine (*Pnma*) structure, which is known as very rare mineral, purpurite, while its iron counterpart, the heterosite ($FePO_4$), is less stable, since $FePO_4$ crystallizes in the α-quartz phase to form the berlinite under normal conditions. From such considerations, we expect that Jahn-Teller distortion effect certainly exists, but it is not the only factor to explain the poor electrochemical performance of $LiMn_yFe_{1-y}PO_4$. One goal of the present work is to address the origins of this poor performance.

The formation of impurity phases will also have an impact on the various properties of these materials. The importance of this issue has been already pointed out for $LiFePO_4$ [10,11]. For instance, the degradation in time of the voltammetric performance of $LiFePO_4$ sample left in the air during few weeks [12] has been associated to the fact that impurity phase may be produced not only during sintering process but also during storage in ambient air [10,13], and results in the aging of the specific capacity [14], due to sensitivity to moisture [15,16]. The same should hold true in the Mn-counterpart, where such an investigation has not been done yet. For this purpose, careful synthesis and the subsequent structural and magnetic analyses of the $LiMn_yFe_{1-y}PO_4$ and $Mn_yFe_{1-y}PO_4$ are needed with an eye to the any trace of impurities and/or residual lithium. In the present article, we carefully prepared a new generation of $LiMn_yFe_{1-y}PO_4$ and $Mn_yFe_{1-y}PO_4$ samples free of any impurities and residual lithium, and revisit prior analyses of their intrinsic magnetic properties.

2. Experimental

Phase-pure $Li(Mn_yFe_{1-y})PO_4$ ($y = 0.2, 0.4, 0.6, 0.8$) powders were synthesized by a solid-state reaction. A stoichiometric amount of lithium carbonate [Li_2CO_3, Wako, >99%], iron(II) oxalate dihydrate [$Fe(II)C_2O_4{\cdot}2H_2O$, JUNSEI, 99%], manganese(II) oxalate hemihydrate [$Mn(II)\ C_2O_4{\cdot}0.5H_2O$, Wako, >99%], and di-ammonium hydrogen phosphate [$(NH_4)_2HPO_4$, Wako, >99%] were used as starting materials. A total of 5 g of raw materials was poured into a 250-mL Cr-hardened SUS container with a mixture of 10 mm in diameter (mm ϕ) × 10 and 5 mm ϕ × 16 Cr-hardened SUS balls and thoroughly mixed by a conventional planetary milling apparatus for 6 h. Then the material was synthesized by sintering at 700 °C for 6 h in a purified argon gas flow.

Chemical oxidation to obtain $(Mn_yFe_{1-y})PO_4$ was performed by reaching $Li(Mn_yFe_{1-y})PO_4$ with nitronium tetrafluoroborate (NO_2BF_4, Alfa Aeser, 96%) in acetonitrile. The redox potential of NO_2^+/NO_2 is about 5.1 V vs. Li^0/Li^+, and it effectively oxidizes $Li(Mn_yFe_{1-y})PO_4$ with redox potential of 3.4 V (Fe^{3+}/Fe^{2+}) and 4.1 V (Mn^{3+}/Mn^{2+}) vs. Li^0/Li^+. After dissolving about 1.6 g of NO_2BF_4, twofold greater than the amount needed for the reaction, into 100 mL of acetonitrile, about 0.8 g of active material was added, and the mixture was stirred for 24 h ($y = 0.2, 0.4, 0.6$) and for 40 h ($y = 0.8$) at room temperature with bubbling of purified argon gas; longer reaction time was needed for $y = 0.8$ to ensure a complete delithiation. The products were filtered several times to remove impurities before drying under vacuum.

X-ray diffraction studies were performed using conventional X-ray diffractometer, Bruker AXS D8 ADVANCE with Bragg-Brentano geometry, which has a sealed Co Kα radiation source (including both Kα1 and Kα2) and linear 1D position sensitive detector (Vantec-1), where Kβ radiation is filtered by Fe foil.

Rietveld refinement was performed using Topas ver. 3.0 software. The refined parameters were lattice constant, fractional atomic coordinates, Lorentzian-type crystallite size broadening, and Gaussian-type strain broadening, while isotropic temperature factor and site occupancy were fixed. Topas employs fundamental parameter approach (FPA), which analytically optimizes the instrument contribution to diffraction profile shapes and refines only diffraction broadening generated by the specimen. Therefore, the refined parameter for coherence length is separated from instrument contribution.

Initial coordinates for $LiMPO_4$ with space group *Pnma* were: Li at 4a ~ (0, 0, 0), Fe at 4*c* (*x*, 1/4, *z*) with *x*; 0.28 and *z*; 0.97, P at 4*c* (*x*, 1/4, *z*) with *x*; 0.10 and *z*; 0.42, O1 at 4*c* (*x*, 1/4, *z*) with *x*; 0.10 and *z*; 0.74, O2 at 4*c* (*x*, 1/4, *z*) with *x*; 0.45 and *z*; 0.20, and O3 at 8*d* (*x*, *y*, *z*) with *x*; 0.16, *y*; 0.05, and *z*; 0.28. Although several types of cation disorder and vacancy modes were considered for refinements, both $LiMPO_4$ and MPO_4 were refined to the stoichiometric compositions. Thermal displacement parameters were assumed to be isotropic and fixed to 1.0 for lithium and oxygen, and 0.6 for

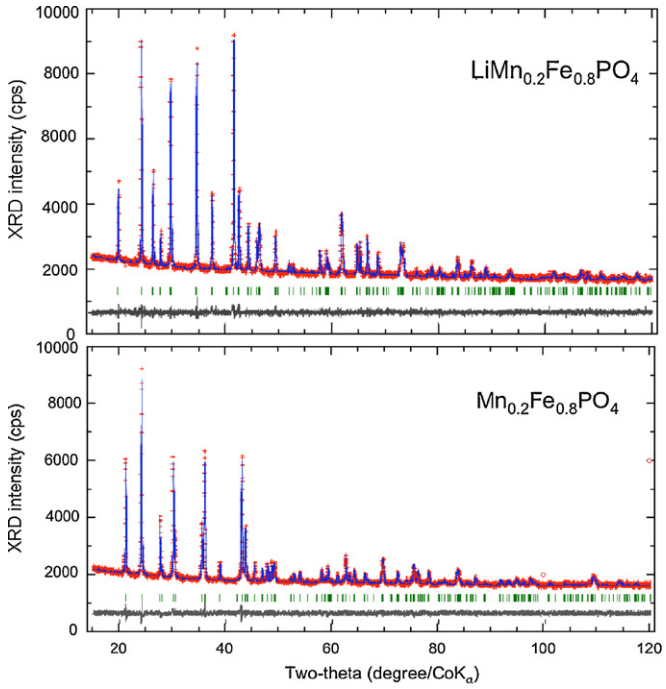

Fig. 2. Rietveld refinement pattern of the X-ray diffraction data of the lithiated and delithiated phases of $Li_xMn_yFe_{1-y}PO_4$ for $y = 0.2$. All the peaks are intrinsic to the olivine structure (*Pnma* S.G.). The observed intensity data are shown by dots. The solid line above overlying them is the calculated intensity. Vertical markers below the diffraction patterns indicate positions of possible Bragg diffractions.

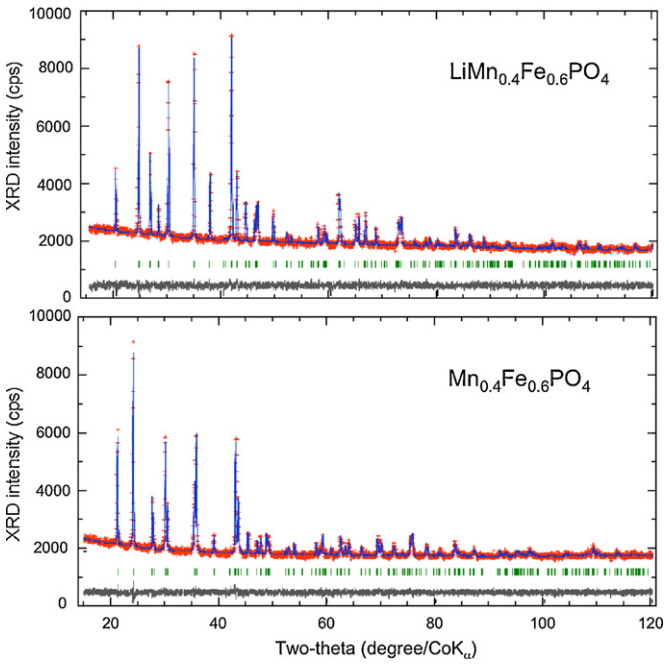

Fig. 3. Same as Fig. 2, for $y = 0.4$. All the peaks are intrinsic to the olivine structure. The lattice distortions associated to Mn^{3+} in the delithiated phase is evidenced by the larger width of the peaks.

iron and phosphorous. Selective distortion around transition metal in $(Mn_yFe_{1-y})PO_4$ system with relatively rigid PO_4 tetrahedra has been reported in the literature [8].

The magnetic measurements (susceptibility and magnetization) were performed with two fully automated SQUID magnetometers (Quantum Design MPMS XL and Quantum Design MPMS-5S) in the temperature range 4–300 K. Powders were placed into small plastic vial, placed in a holder and finally inserted into the helium cryostat of the SQUID apparatus. The temperature dependence of the susceptibility data was recorded during heating of the sample using two modes: zero-field cooling (ZFC) and field cooling (FC), to determine the magnetic behaviour. The procedure is based on performing two consecutive magnetization measurements: in ZFC the sample is first cooled down in the absence of magnetic field, then a magnetic field $H = 10$ kOe is applied, and the ZFC magnetic susceptibility $M(T)/H$ where M is the magnetization is measured upon heating. In the FC experiments, the same magnetic field is applied first at room temperature; the FC susceptibility is measured upon cooling. No difference, i.e. no magnetic irreversibility effect has been detected between ZFC and FC measurements in any of the samples. Magnetic curves $M(H)$ have been measured in an applied magnetic field in a range 0–30 kOe.

3. Results and discussion

3.1. Characterization

The XRD pattern is illustrated for $Li_xMn_yFe_{1-y}PO_4$ samples with compositions $y = 0.2$, 0.4 and $y = 0.8$ in Figs. 2–4, respectively, both in the lithiated ($x = 1$) and delithiated ($x = 0$) phases. All Bragg lines are indexed in the orthorhombic system (*Pnma* S.G.). Both the Li and M atoms are in octahedral sites with Li located in the 4*a* and M in the 4*c* positions. The refined lattice parameters are in agreement with values reported previously in the literature [8]. Additionally, the profiles of the Bragg lines are narrow and symmetric. The lattice parameters increase linearly with the composition *y* in $LiMn_yFe_{1-y}PO_4$ [8]. The main effect of the substitution of Fe by Mn in $LiMn_yFe_{1-y}PO_4$ is then a dilatation of the lattice, which can be simply explained by the difference in ionic radii of high-spin Mn^{2+} (0.97 Å) and high-spin Fe^{2+} (0.92 Å) [8]. The situation is different in $Mn_yFe_{1-y}PO_4$. The variations of the lattice parameters with *y* in this case are reported in Fig. 5. The *c*-parameter is roughly independent of *y*, while *b* increases with *y*, but now *a* decreases with *y*. Therefore, the substitution of Fe^{3+} by Mn^{3+} mainly results in the deformation

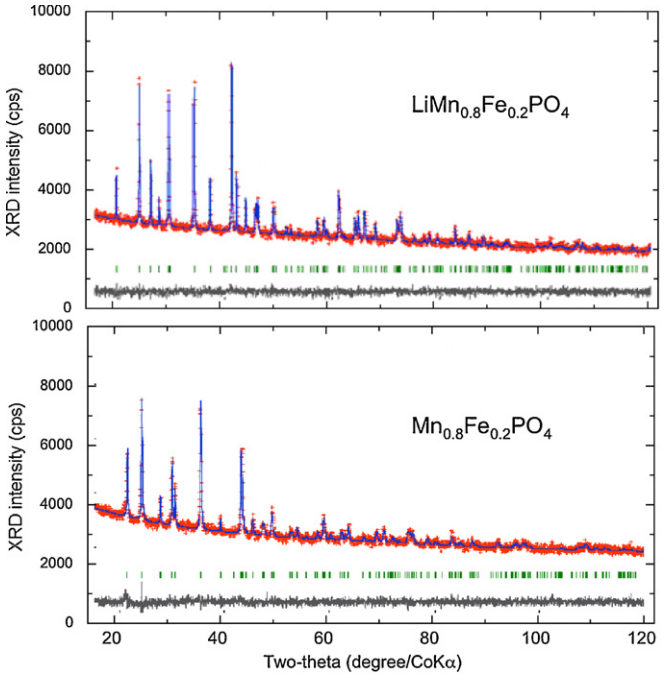

Fig. 4. Same as Fig. 2, for $y = 0.8$. All the peaks are intrinsic to the olivine structure. The lattice distortions associated to Mn^{3+} in the delithiated phase is evidenced by the larger width of the peaks.

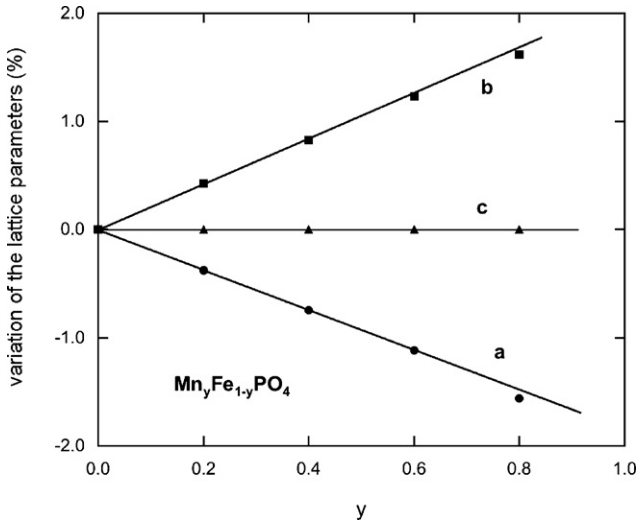

Fig. 5. Relative variations of the lattice parameters of $Mn_yFe_{1-y}PO_4$ as a function of y. Note the smaller values of a and b parameters for the $y = 0.8$ case, with respect to the linear interpolation from the data at $y < 0.8$. This departure from the Vegard's law at $y = 0.8$, although small is significant, and best evidenced by the reduction of the volume of the unit cell in Fig. 7.

of the lattice, which increases with the Mn-content y. The variations $\Delta V/V$ of the unit cell volume with y are reported in Fig. 6. $\Delta V/V$ increases with y in the range $0 \le y \le 0.6$, and this increase is linear in y, within the experimental uncertainty (also reported in the figure). Surprisingly, however, further increase of y from 0.6 to 0.8 leads to a decrease of the volume of the unit cell, instead of an increase. Magnetic measurements will show us that this anomaly is attributable to a spin-transition of a fraction of the Mn^{3+} ions from the high-spin to the low-spin state.

In general, several factors can contribute to the broadening of peaks in X-ray diffraction [17,18]. We have already shown that we cannot neglect the strain contribution in manganese compounds [19]. We then follow this previous work and combine the Scherrer's equation and the Bragg's law for diffraction to determine crystallite size L and micro-strain local $\langle e^2 \rangle$ by using the following equation

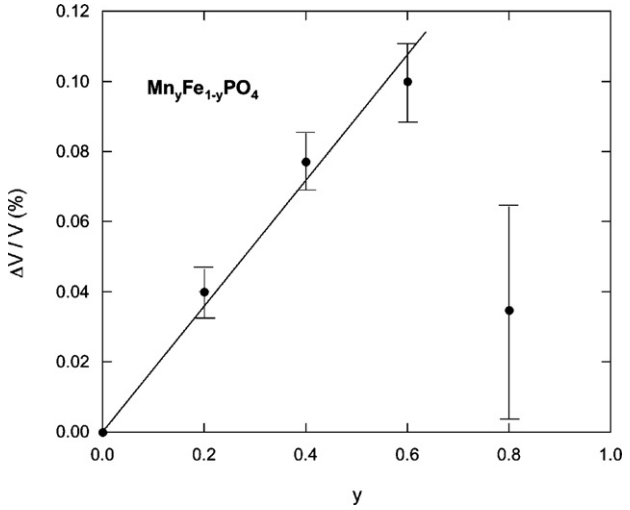

Fig. 6. Relative variation of the volume of the unit cell in $Mn_yFe_{1-y}PO_4$ as a function of y. The larger error bar for the $y = 0.8$ case due to the lower quality of the Rietveld refinement for this sample. The straight line is a guide for the eye and illustrates the linear variations expected from the Vegard's law that is distinctly violated at $y = 0.8$.

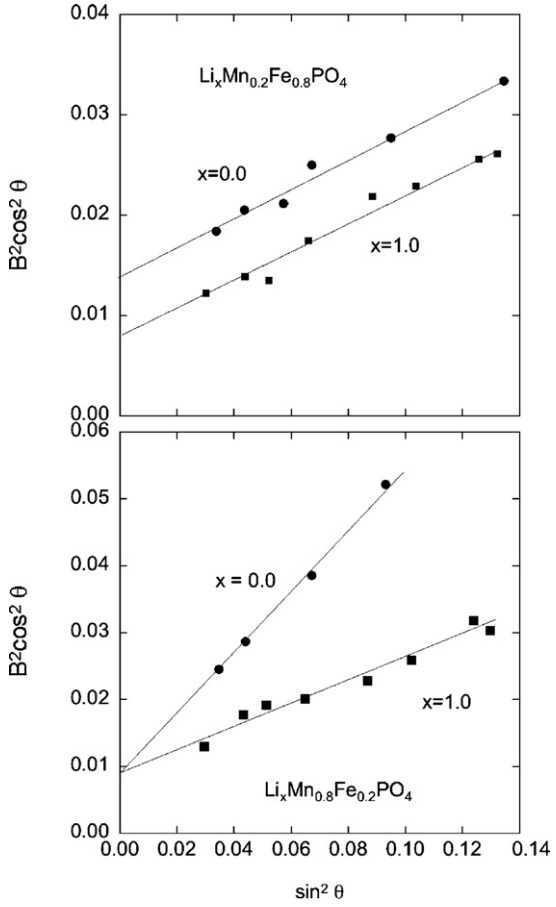

Fig. 7. Analysis of the full-width B at half-maximum of the XRD peaks, according to Eq. (1). Note B is in degree (not radian) here, to make contact with the XRD spectra in Figs. 2–4.

[19]:

$$B^2 \cos^2\ \theta = 16\langle e^2 \rangle \sin^2\ \theta + \frac{K^2\lambda^2}{L^2}, \quad (1)$$

where B is the full-width at half-maximum (fwhm) in radian, after correction of the instrumental broadening for finely powdered silicon powder, q is the diffraction angle, and K is a near-unity constant related to crystallite shape. The plot of the first member as a function of $\sin^2\theta$ is reported in Fig. 7 for two cases $y = 0.2$ and 0.8. The plots are well fit by straight lines, in agreement with Eq. (1). The slope of the linear fit of the data provides us with the value of $\langle e^2 \rangle$, while the extrapolation to $\sin\theta = 0$ provides us with the value of the coherence length L.

Note the linear law evidenced in the figure gives indirect evidence that L is independent of θ. The crystallites are then spherical in first approximation, so that we take for the constant K the value appropriate to this particular case, namely $K = 0.9$. The spatial coherence length of samples of given composition may vary by a factor two from one sample to another, due to the impossibility to control all the numerous parameters during the synthesis process. Therefore, the dependence of L on y is meaningless. However, for all the samples we have investigated, we find $L \approx 100$ nm within a factor two, quite comparable to the coherence length reported in the literature for well-crystallized $LiFePO_4$ [20]. On another hand, the variation of L for a given sample (at given y) upon delithiation is meaningful. For $y \le 0.6$, we find L is reduced after full delithiation. For the particular case sample ($y = 0.2$) in Fig. 7a, we find $L = 132$ nm for $x = 1.0$, decreasing to 80 nm for $x = 0$. On another hand, we find that $\langle e^2 \rangle$ is unaffected by the delithiation process in the whole range

of Mn compositions $y \leq 0.6$. Therefore, the lattice can accommodate the valence change of the Mn ions without generating local strain fields. This is the proof that all the Mn^{3+} ions have the same ionic radius, i.e. are in the same state (we shall find from magnetic measurements that they are in the high-spin state). In such a case where all the magnetic ions have the same ionic radius, the periodicity of the lattice is maintained, so that the change $Mn^{2+} \rightarrow Mn^{3+}$ generates uniform strain fields entirely accommodated by the global distortion of the lattice, evidenced by the variations of the lattice parameters investigated above, and the formation of extended defects that reduce the lattice coherence length L.

To the contrary, in the case $y = 0.8$, Fig. 7b shows that the delithiation leads to an important increase in $\langle e^2 \rangle$ while the coherence length is not significantly affected ($L = 100$ nm), meaning that local strain fields are generated in the delithiation process. Again, this outstanding result is due to the fact that an important fraction of Mn^{3+} (we shall see in the next sections that this fraction is 20%) is in the low-spin state. Besides the lattice distortion that accommodates the averaged strain resulting from the valence change $Mn^{2+} \rightarrow Mn^{3+}$, local strain fields are generated by the Mn^{3+} ions in the low-spin state that behave like 'impurities', since their ionic radius is not the same as that of Mn^{3+} in the high-spin state.

This result is consistent with the hitherto reported tendencies: (i) delithiation kinetics become slow and complete reaction is much difficult for Mn-rich phase. (ii) The increase of the local strain fields upon delithiation, as measured by the increase of $\langle e^2 \rangle$ from $x = 1$ to $x = 0$, is important at $y > 0.6$, and actually it exceeds the limit that the lattice can afford when the Mn concentration exceeds $y = 0.8$. The X-ray diffraction signal almost disappears at $x < 0.2$ in Li_xMnPO_4 [2,4,5,8]. The case $y = 0.8$ is then the composition with the largest value of y for which the complete chemical delithiation has been possible in this triphylite family. This is consistent with the fact that the complete delithiation of the $y = 0.8$ case required much longer reaction times and longer stirring, as mentioned in Section 2. The results of the Rietveld refinement for this particular case are illustrated in Table 1. For this particular composition, the results are different from those of Ref. [8], and the lattice parameters (in the table caption) smaller than in Ref. [8]. This is evidence that the delithiation of $LiMn_{0.8}Fe_{0.2}PO_4$ was not complete in Ref. [8], and an additional proof will be provided by the analysis of the magnetic properties reported below. On another hand, the Rietveld results for the other samples, delithiated or not are in agreement with the results reported in [8]. The results in Table 1 show that the quality of the Rietveld refinement is lower for the $Mn_{0.8}Fe_{0.2}PO_4$ than in the other samples [8]. This is again the evidence of the lower crystallinity of this sample resulting not from the coherence length that is still large, but from the local micro-strains and local deformations.

3.2. Optical properties

The FTIR spectra are reported in Figs. 8 and 9 for the samples of the series $x = 0$ and $x = 1$, respectively. For $x = 1$, the FTIR spectra are in continuity with that of $LiFePO_4$ reported before [21,22]. The only change is a small shift of the bands at low frequency (wavenumber $\sigma < 700\ cm^{-1}$) as a function of y, due to the variation of the lattice parameter that modifies the (Mn, Fe)—O bond strength and thus the external modes, or lattice vibrations, responsible for this part of the spectra. On another hand, the shift of the vibration modes is smaller for the high frequency part of the spectrum at $\sigma > 800\ cm^{-1}$, because these are internal modes associated to vibrations of the PO_4 units, and the strongly covalent P—O bond is not significantly affected by the substitution of Fe by Mn.

This holds also true for the evolution of the FTIR spectra of the delithiated samples ($x = 0$) as a function of y provided $y < 0.8$. We find that the spectra are in continuity with that of $FePO_4$ [23]. However, there is an extra line at 291 cm^{-1} in the $x = 1$ that does not exist for $x = 0$, which is thus associated to the vibration of the lithium ion. To identify this mode, we note that the isotopic ^6Li–^7Li sub-

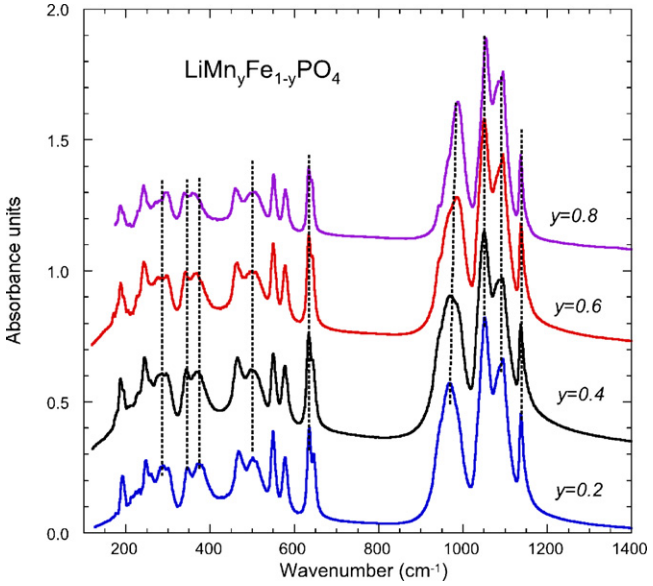

Fig. 8. FTIR spectra of $LiFe_yMn_{1-y}PO_4$. Broken lines are guides are the eyes to follow up the bands as a function of the composition.

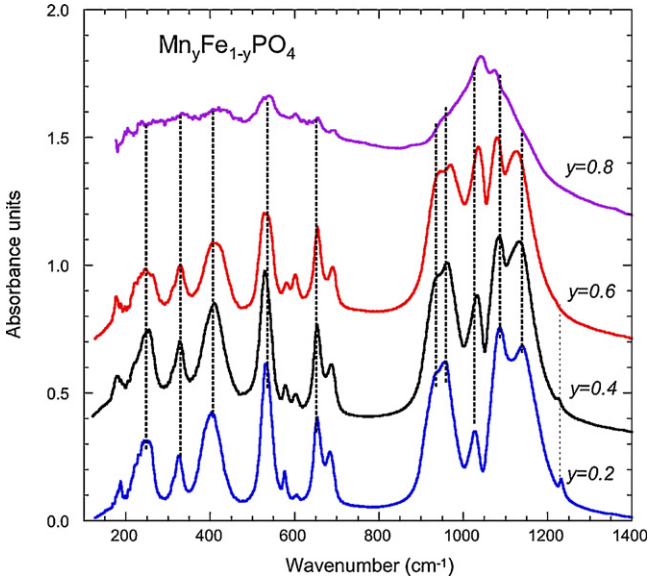

Fig. 9. Same as Fig. 4, after delithiation for $Mn_yFe_{1-y}PO_4$ samples.

Table 1
Rietveld refinement results for $Mn_{0.8}Fe_{0.2}PO_4$.

Atom	Site	x	y	z	B (Å)
Fe, Mn	4*c*	0.2826(6)	0.25	0.924(1)	0.6
P	4*c*	0.0974(8)	0.25	0.387(2)	0.6
O1	4*c*	0.123(2)	0.25	0.711(3)	1
O2	4*c*	0.437(2)	0.25	0.153(3)	1
O3	8*d*	0.166(1)	0.032(2)	0.237(2)	1

The lattice parameters are $a = 9.657(1)$, $b = 5.8797(5)$, $c = 4.7755(5)$. R-parameters of the refinement are $R_{exp} = 1.242$, $R_{wp} = 1.327$, $R_p = 1.044$, while the goodness of fit (GOF) is = 1.068.

stitution in lithiated dioxides of transition metals has proven the asymmetric stretching vibrations of LiO_6 to occur in the far-infrared region (below 300 cm^{-1}) [24]. In particular, this mode in the same O_h configuration has been observed at 260 cm^{-1} in $LiCoO_2$, and at 240 cm^{-1} in $LiNiO_2$ [24]. The line at 291 cm^{-1} in our samples with $x = 1$, only shifted by few cm^{-1} with respect to $LiCoO_2$, corresponds to this same cage mode of the lithium ions that undergo translation vibrations inside the cage formed by the six nearest neighbor oxygen atoms. Therefore, the absence of this line at 260 cm^{-1} in the spectrum of $Mn_yFe_{1-y}PO_4$ is a direct proof that these samples have been completely delithiated. With respect to XRD, we note that the FTIR is a probe of the composition of the samples at a much more local scale, and in addition, the presence of this peak specific to Li upgrades the FTIR spectroscopy to a method of detection of zero-Li concentration. The FTIR is then more sensitive than XRD to detect the presence of Li. We shall see the importance of this property in the next section on magnetic properties.

The FTIR spectra of the delithiated samples in Fig. 9 also show a large change of the intensities of the band at 1030 cm^{-1}. The reason is that, upon delithiation, the iron oxidizes first. The smaller ionic radius of Fe^{3+} (0.78 Å) with respect to that of Fe^{2+} (0.92 Å) implies a static distortion. Moreover, Jahn-Teller distortion of the MO_6 octahedra are expected, which will be stronger upon oxidation of the manganese, and will increase with the Mn concentration, since Mn^{3+} is also known to be a Jahn-Teller ion. This distortion affects the symmetry of the stretching P–O–P mode of the PO_4 units, since the oxygen ions are shared with MO_6 octahedra (see Fig. 1). The result is the increase in intensity (in addition of a shift in energy) of the corresponding band circa 1030 cm^{-1} in the spectra as the Mn concentration increases. This feature is then an indirect evidence of the Jahn-Teller distortion of the octahedra, through its effect on the vibrations of the PO_4 units. Note the relative intensities of the FTIR are not sensitive to the Mn concentration in the $x = 1$ samples (see Fig. 8), the proof that the strong Jahn-Teller distortion is indeed generated by the delithiation. This result is actually consistent with the decrease of the XRD coherence length upon delithiation, which we have evidenced in the previous section.

The FTIR spectrum of $Mn_{0.8}Fe_{0.2}PO_4$ is markedly different from the others, since the bands are broadened. This broadening shows that the lifetime of the phonons has become much smaller due to their diffusion by local lattice distortions. Actually the broadening is so important that the width of the FTIR bands is comparable to the one that we have observed in amorphous $LiFePO_4$ [25–27]. The XRD spectra, however, are quite different: no XRD peak and amorphous halo in the glassy state [26], well resolved XRD peaks in $Mn_{0.8}Fe_{0.2}PO_4$. Let us recall that the spatial coherence length deduced from the XRD analysis is 9 nm, and then remains very large with respect to the inter-atomic distance. $Mn_{0.8}Fe_{0.2}PO_4$ is then well crystallized in the olivine structure. The type of disorder evidenced here is then quite different from that we met in the glassy state. In both cases the broadening of the FTIR spectra is the signature of the distortion of the molecular edifices, but not at all at the same length scale: loss of long-range spatial order due to ill-crystallization in Refs. [25–27], local Jahn-Teller distortions that keep long-range atomic order here. Therefore, the FTIR plus XRD experiments on $Mn_{0.8}Fe_{0.2}PO_4$ give evidence that the local and randomly distributed Jahn-Teller distortions are quite important, so that locally, the random crystal fields are comparable to the ones encountered in the glass state, but still the long-range crystal order is preserved on average. $Mn_{0.8}Fe_{0.2}PO_4$ then gives a rare example of a solid at the verge of instability, and provides us with some enlightenment on the fact that the material becomes amorphous upon delithiation at $x < 0.2$ as soon as the Mn concentration is larger [2,4,5,8]. Our results also suggest that the FTIR spectroscopy is actually more sensitive than X-ray absorption spectroscopy to detect random distortions in crystals [28].

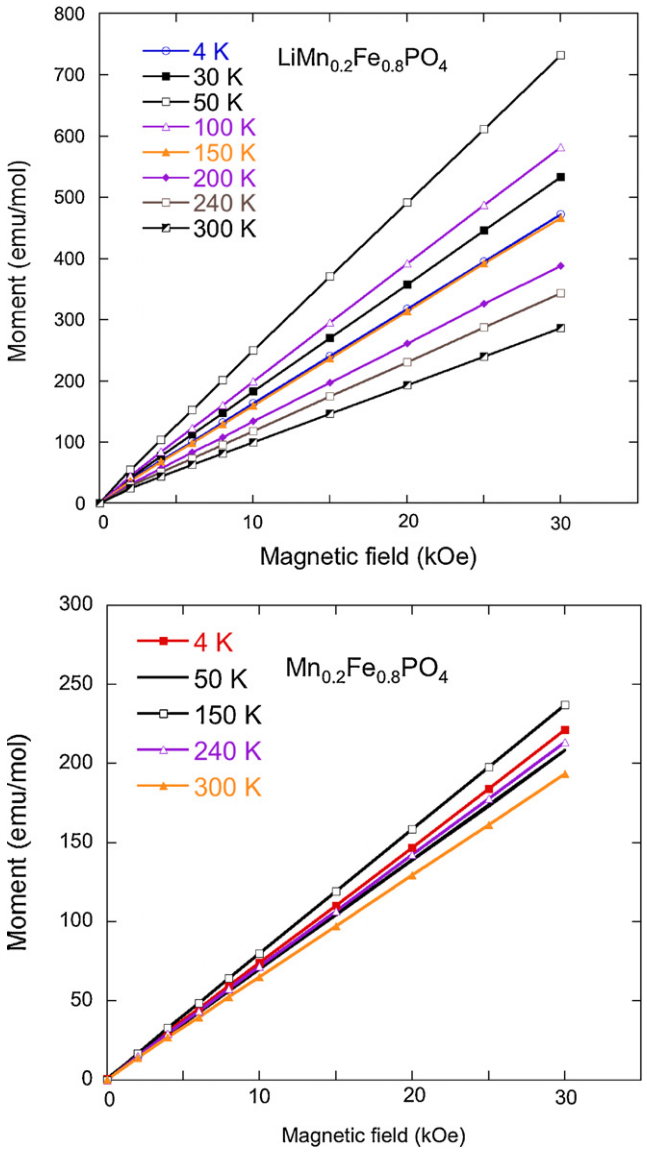

Fig. 10. Magnetization curves for the composition $y = 0.2$ before and after delithiation.

3.3. Magnetic properties

Measurements of the isothermal magnetization curves $M(H,T)$ show a linear relationship $M(H,T) = \chi(T)H$ that indicates the absence of ferro- or ferri-Fe-based magnetic impurities that can poison these materials [10,13,25,29] and Mn-based impurities as well [30]. This is illustrated in Fig. 10 for one composition $y = 0.2$ chosen as an example but this holds true for all the samples investigated in this work. The temperature dependence of the inverse of the magnetic susceptibility $\chi^{-1}(T)$ is reported in Fig. 11 for the lithiated ($x = 1$) and fully delithiated ($x = 0$) samples.

At high temperature, the variations of χ^{-1} are linear in H, which means that the Curie–Weiss law is satisfied:

$$\chi(T) = \frac{C_p}{T + \theta_p}, \quad (2)$$

with θ_p the Weiss temperature. The intrinsic effective magnetic moment μ_{eff} carried by Fe^{2+} and Mn^{2+}, is deduced from the Curie

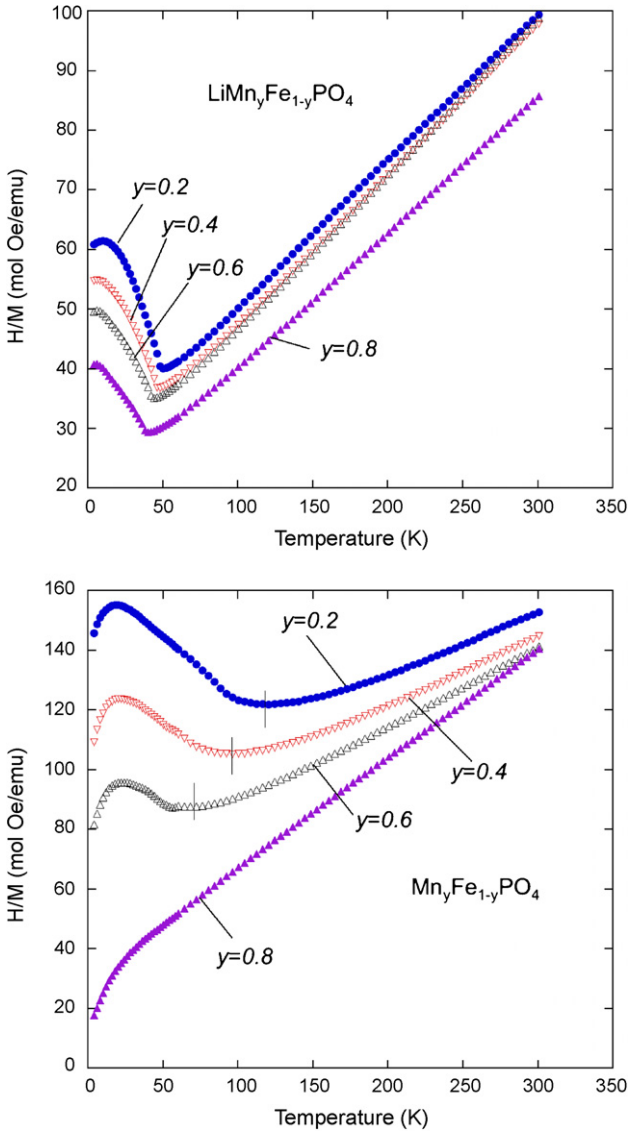

Fig. 11. Inverse of the magnetic susceptibility as a function of temperature for lithiated and delithiated samples. Vertical lines point to the Néel temperature.

constant according to the relation:

$$C_p = \frac{N\mu_{\text{eff}}^2}{3k_B}, \tag{3}$$

with N the number of magnetic ions and k_B the Boltzmann constant. The theoretical value of the magnetic moment for lithiated and delithiated samples is given by

$$\mu_{\text{eff}} = [(1-y)\mu_{\text{Mn}^{2+}}^2 + y\mu_{\text{Fe}^{2+}}^2]^{1/2} \quad \text{if } x = 1, \tag{4}$$

$$\mu_{\text{eff}} = [y\mu_{\text{Fe}^{3+}}^2 + (1-y)\mu_{\text{Mn}^{3+}}^2]^{1/2} \quad \text{if } x = 0. \tag{5}$$

We have argued elsewhere [10,25] that the effective magnetic moments carried by the magnetic ions correspond to the spin only value, because the crystal field quenches the orbital momentum, so that:

$$\mu_{\text{Fe,Mn}} = 2\mu_B[S_{\text{Fe,Mn}}(S_{\text{Fe,Mn}}+1)]^{1/2}. \tag{6}$$

Shown in Figs. 12 and 13 are experimental values of μ_{eff} deduced from Eq. (3) for $x = 1$ and $x = 0$ samples, respectively. The theoretical effective magnetic moments are also reported for comparison. They have been calculated from Eqs. (4) and (5) assuming that all

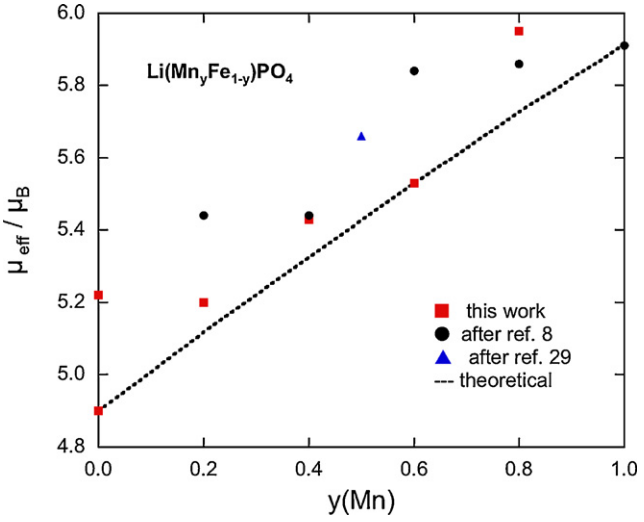

Fig. 12. Effective magnetic moment per magnetic ion for LiMn$_y$Fe$_{1-y}$PO$_4$ samples in this work, and prior works.

the magnetic ions are in the high-spin state. For $x = 1$, it means $\mu(Fe^{2+}) = 4.9\,\mu_B$ and $\mu(Mn^{2+}) = 5.9\,\mu_B$, corresponding to $S = 2$ and $S = 5/2$, respectively, in Eq. (6). For $x = 0$, it means $\mu(Fe^{3+}) = 5.9\,\mu_B$ and $\mu(Mn^{3+}) = 4.9\,\mu_B$, corresponding to $S = 5/2$ and $S = 2$.

In LiMn$_y$Fe$_{1-y}$PO$_4$, the experimental value is either in quantitative agreement with the theoretical value, or slightly larger. It confirms that both Mn^{2+} and Fe^{2+} are in the high-spin state. We know from earlier works that samples without any defect have an effective moment in quantitative agreement with the theoretical value. This is the case here for the $y = 0.6$ sample, and we have also found that the effective magnetic moment of Fe^{2+} in the $y = 0$ samples may vary in the range 4.9 (that is the theoretical value) and 5.22 μ_B. We have shown recently that this excess of magnetic moment in such a case is due to the contribution of the magnetic small polarons associated to few Li vacancies, in concentration below 1% [31]. As samples in this study were treated carefully, the experimental values of μ_{eff} for the different samples tend to be closer to the theoretical values than prior results previously reported in the literature.

In Mn$_y$Fe$_{1-y}$PO$_4$, the experimental value of the effective magnetic moment is also in reasonable agreement with the theoretical one, except for the $y = 0.8$ case, where μ_{eff} is dramatically lower than

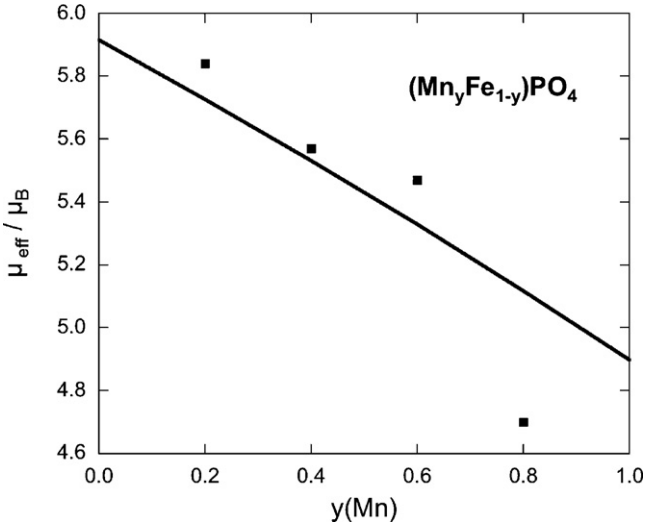

Fig. 13. Effective magnetic moment per magnetic ion for LiMn$_y$Fe$_{1-y}$PO$_4$.

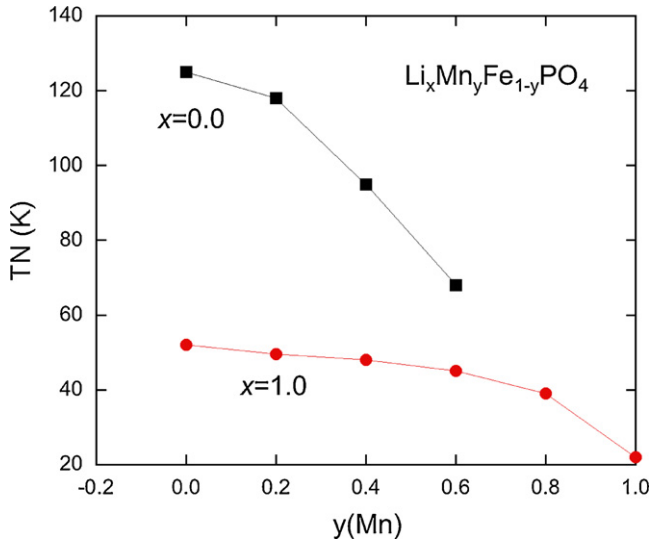

Fig. 14. Variation of the Néel temperature as a function of the composition y in $Li_xMn_yFe_{1-y}PO_4$ for $x = 0$ and $x = 1$.

expected. This shows that in this particular case, part of the Mn^{3+} ions have switched to the low-spin state $S = 1$ (effective moment 2.83 μ_B), which is the spin-configuration adopted by manganese when it is submitted to a strong crystal field in the octahedral symmetry. The experimental value $\mu_{eff} = 4.7\ \mu_B$ for this sample means that about 1/3 of the Mn^{3+} ions is in the low-spin state, 2/3 are in the high-spin state. To be more precise, we find that the amount of Mn^{3+} in the high-spin state per chemical formula is 0.54, a figure close to 0.6. This result has to be linked with the fact that both the structural and magnetic properties show the Mn^{3+} ions in $Mn_{0.6}Fe_{0.4}PO_4$ are still in the high-spin state. Therefore, we can conclude that $y = 0.6$ is the highest Mn concentration where the chemical delithiation can be completed without the spin-transition of Mn^{3+} ions in the low-spin state. If the Mn concentration y increases beyond this limit, the additional Mn^{3+} ions generated by the delithiation process have to undergo a transition to the low-spin state.

The magnetic susceptibility of the lithiated samples goes through a maximum at the Néel temperature T_N corresponding to the transition from the paramagnetic to the antiferromagnetic (AFM) phase. T_N is an increasing function of y, ranging from $T_N = 22$ K in $LiMnPO_4$ to $T_N = 52$ K in $LiFePO_4$ [32]. The $T_N(y)$ curve, however, is far from linear, due to the fact that exchange interactions involve overlap integrals between the d-electron metal states and p-oxygen states, which do not decrease linearly with the M–O distance.

The delithiation process results in an increase of T_N. This is actually expected since the heterosite ($FePO_4$) is strongly antiferromagnetic with Néel temperature $T_N = 130$ K. This can be viewed on Fig. 14 where the $T_N(y)$ curve for the $x = 0$ samples has also been reported for comparison with the $x = 1$ case. On another hand, the magnetic susceptibility curve does not go through a maximum at any temperature investigated in $Mn_{0.8}Fe_{0.2}PO_4$ so that this sample does not order antiferromagnetically, at least in the temperature range we have explored ($T > 4$ K). This is at contrast with a previous result, according to which such a sample would undergo a transition to the antiferromagnetic order at $T_N \approx 50$ K just like the $y = 0.6$ delithiated sample [8]. Actually, the monotonic decrease of T_N with y shows that T_N would be approximately 20 K in the $Mn_{0.8}Fe_{0.2}PO_4$ sample. This is also the value of T_N predicted if the ratio between T_N and θ_p is the same in the $y = 0.8$ and the $y = 0.6$ samples, which is a reasonable assumption since the magnetic exchange paths are the same in both samples. The existence of the minimum at $T_N \approx 50$ K in the $y = 0.8$ sample of Ref. [8] is then the sign that the sample has not been completely delithiated, since this Néel temperature compares well with the Néel temperature of the lithiated phase ($T_N \approx 40$ K for $LiMn_{0.8}Fe_{0.2}PO_4$). This is actually self-consistent with the structural properties reported earlier in this work, as the lattice parameters of $Mn_{0.8}Fe_{0.2}PO_4$ are smaller than those of the sample in Ref. [8]. It does not explain, however, that no antiferromagnetic ordering is observed in the $Mn_{0.8}Fe_{0.2}PO_4$ sample of the present work even below 20 K. We have already met this situation in $LiFePO_4$ prepared under such conditions that the coherence length of the lattice was at the molecular scale [25,27]. In the present case, however, the coherence length (100 nm for this sample) is large enough to insure that long-range spin-correlation can develop to generate the antiferromagnetic ordering. One possible explanation is that 20 K is the typical temperature at which the loose impurity spins that are always present in such samples dominate the magnetic properties. This can be viewed in Fig. 11 by the fact that, for all the samples undergoing a transition to the antiferromagnetic ordering at a larger temperature, χ^{-1} does not increase upon cooling down to $T = 0$ as it is expected for antiferromagnets, but actually decreases below 20 K due to the Curie contribution of such loose spins to the magnetic susceptibility (that diverges in T^{-1}, and then overcomes the intrinsic part at low temperature, even if the concentration of loose spins is small). Therefore, the minimum in the $\chi^{-1}(T)$ curve at T_N may be masked by the dominant contribution of the loose spins in $Mn_{0.8}Fe_{0.2}PO_4$. The report that purpurite ($MnPO_4$) is a non-magnetic mineral [33] is not a proof either that the material does not order antiferromagnetically at 20 K or below, because the mineralogists define "non-magnetic" as a material that is not ferromagnetic. We did not observe spin–glass freezing either. In particular, no magnetic irreversibility, i.e. no difference between field-cooled and zero-field-cooled experiments has been detected in our experiments. The main reason is that the spin–glass transition in frustrated systems is favored by spin-dilution [34,35], while we are dealing here with non-diluted spin systems: even in its low-spin state, Mn^{3+} still carries a spin $S = 1$.

In the type of materials we have, the Curie–Weiss law is valid in the range $T \geq 2T_f$, with T_f the spin-freezing temperature [36]. In the material investigated here, $T_f \equiv T_N$. Since T_N is smaller than 100 °K for all the samples except in $Mn_{0.2}Fe_{0.8}PO_4$, the Curie–Weiss law is well satisfied in the temperature range $200 < T < 300$ K used to fit the data. In the particular case ($x = 0$, $y = 0.2$), however, $T_N = 120$ K (see Fig. 11), so that the temperature range $T > 2\theta$ is reduced to 240–300 K. This shorter range results in a large uncertainty on the value of θ, a situation we have already met in $Li_{1+x}Mn_{2-x}O_4$ [30]. On another hand, the error on μ_{eff} in $Mn_{0.2}Fe_{0.8}PO_4$ is the order of 1%, which is negligible since the variations of μ_{eff} as a function of y are as large as 20%. Note, however, that θ can be determined unambiguously for the most interesting case $x = 0$, $y = 0.8$, because then, the transition to the low-spin state has depressed the spin-freezing temperature: $\theta = 81$ K, much smaller than in all the other samples where the manganese is in the high-spin state. This is actually expected since, in a homogeneous material, $\theta \propto S(S+1)$ varies like the square of the spin.

The spin-transition of manganese between high-spin and low-spin states also happens in some Mn-chalcogen compounds. It does not happen in MnO_2 because the manganese stays in the Mn^{4+} configuration that prevents such a transition. It has been observed, however, with oxygen replaced by other chalcogen atoms, such as MnS_2 [37] and $MnTe_2$ [38,39] since Mn is in the 2+ oxidation state. In such materials where the lattice parameter cannot be changed by lithiation or delithiation, the variation of the lattice parameters needed to obtain this transition has been achieved by applying pressure. In these cases, the lattice distortion that accompanies the spin-transition (the analog of the Jahn-Teller distortion in our compounds) is the structural transformation from pyrite to marcasite that can be viewed as an orthorhombic distortion of the cubic pyrite

structure. Closer to our system are $CsMnF_4$ [40] and $ZnMn_2O_4$ [41], since the spin-transition in these systems is observed with Mn ions in the same oxidation state. In essence, the spin-transition we have met in our material is then analog to that of other compounds of transition metals where it has been observed, and has the same origin: crystal field plus strong lattice distortion. The difference, however, comes from the origin of the distortion. The solid compounds where the transition has been investigated in the literature are homogeneous materials, which means that the lattice distortion is uniform and can be viewed as a cooperative Jahn-Teller distortion, while in our case, the distortion is local as it occurs upon delithiation, as already discussed in the section devoted to the analysis of FTIR experiments, which also means randomness in the electric (crystal field) and magnetic (exchange) interactions between the magnetic ions. This randomness will actually impact the physical properties. First it implies that all the Mn ions are no longer equivalent, so that only a part of them switch to the low-spin state (we have estimated this fraction to 1/3). The second, and more important consequence is that the spin-transition will not generate charge density waves or any other exotic magnetic ordering that is sometimes observed in homogeneous cases, because the material will actually belong to the different class of magnetic materials known as the family of random-field systems.

3.4. Electrochemical properties

Fig. 15a and b shows the typical electrochemical features of Li cells with $LiMn_yFe_{1-y}PO_4$ positive electrodes, i.e. the voltage profile of the first charge discharge for $y = 0.5$ at two C-rate (C/24 and 1C) and the capacity as a function of composition y at 1C-rate.

Note the excess in magnetic moment in Figs. 11 and 12 shows that the concentration of small polarons [31] is almost independent of the Mn concentration. The three to four orders of magnitude difference in the electronic conductivity of $LiMnPO_4$ and $LiFePO_4$ [6] is thus due to the huge difference in the electronic mobility itself. This is simply due to the fact that the activation energy for polaron hopping is much larger in $LiMnPO_4$ (1 eV, against 0.6 eV in $LiFePO_4$). The rate-limiting factor in Li_xMPO_4 is the electronic conductivity rather than the ionic conductivity that is intrinsically large in olivine systems [42]. Then, we can simply expect much larger polarization upon charge–discharge for Mn-rich phases. This is indeed what is observed in this work and in Refs. [2,43,44]. It follows that electrode activity of Mn-rich $LiFe_yMn_{1-y}PO_4$ cannot be significantly improved. In addition, we have found that the delithiation process reduces the coherence length of the lattice, and thus generates dislocations and grain boundaries that are not reduced in the end members. This is a major difference with the case of $LiFePO_4/FePO_4$ system where we found that the crystal recovery was achieved due to a superplastic process [45]. The variation of the lattice parameter that modifies the Mn—O bond strength combined with the Jahn-Teller lattice distortion associated to Mn^{3+} (that does not exist with Fe^{3+}) are responsible for an irreversible plastic deformation in $Li_xFe_yMn_{1-y}PO_4$, hence an aging of this cathode upon cycling. These combined effects of much larger polarization upon charge–discharge and aging will impede the potential use of Mn-rich $LiFe_yMn_{1-y}PO_4$ as a future cathode element for lithium batteries, unless the particle size will be decreased to the nanoscale. In addition, both the structural and the magnetic properties give evidence that the Mn^{3+} ions that are generated by the delithiation remain in the high-spin state up to a concentration $y_c = 0.6$ per chemical formula, only. Beyond this limit, the Mn^{3+} ions in excess switch to the low-spin state. This spin-transition that severely affects the magnetic properties has impact also on the structural properties since it reduces the volume of the unit cell. The additional effects of strong lattice distortion upon substitution of Fe by Mn, and the contraction of the lattice upon spin-transition of the

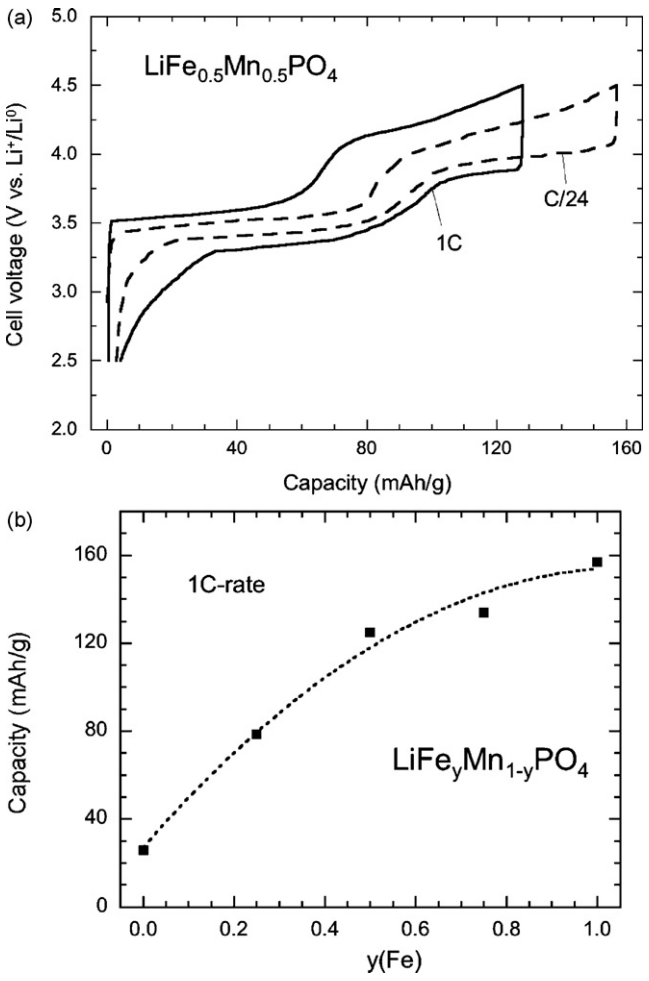

Fig. 15. (a) The voltage profile of the first charge discharge at two C-rate (C/24 and 1C) for cells with $LiMn_{0.5}Fe_{0.5}PO_4$ positive electrodes and (b) the capacity as a function of y(Fe) composition at 1C-rate.

Mn^{3+} in excess of y_c prevent the Li^+ ions from diffusing. As a consequence, it is very difficult to delithiate $LiFe_yMn_{1-y}PO_4$ with $y = 0.8$ (since it amounts to create a concentration of 0.2 Mn^{3+} in the low-spin state besides the Mn^{3+} in the high-spin state in concentration y_c per chemical formula), and we found impossible to delithiate samples with higher content in manganese. We then conclude that $y_c = 0.6$ is a maximum in the composition of the triphylite for best use as a cathode element.

References

[1] A.K. Padhi, K.S. Nanjundaswamy, J.B. Goodenough, J. Electrochem. Soc. 144 (1997) 1188.
[2] M. Yonemura, A. Yamada, Y. Takey, Y. Sonoyama, R.J. Kanno, Electrochem. Soc. 151 (2004) A1352.
[3] M. Piana, B.L. Cushing, J.B. Goodenough, N. Penazzi, Solid State Ionics 175 (2004) 233.
[4] A. Yamada, S.C. Chung, J. Electrochem. Soc. 148 (2001) A960.
[5] A. Yamada, Y. Kudo, K.-Y. Liu, J. Electrochem. Soc. 148 (2001) A1153.
[6] K. Rissouli, K. Benkhouja, J.R. Ramos-Barrado, C.M. Julien, Mater. Sci. Eng. B 98 (2003) 185.
[7] K. Zaghib, A. Mauger, J.B. Goodenough, F. Gendron, C.M. Julien, Chem. Mater. 19 (2007) 3470.
[8] A. Yamada, Y. Takei, H. Koizumu, N. Sonoyama, R. Kanno, Chem. Mater. 18 (2006) 804.
[9] H.-Y. Meethong, S. Huang, A. Speakman, W.C. Carter, Y.-M. Chiang, Adv. Funct. Mater. 17 (2007) 1115.
[10] C.M. Julien, A. Mauger, A. Ait-Salah, M. Massot, F. Gendron, K. Zaghib, Ionics 13 (2007) 395.
[11] A. Ait-Salah, A. Mauger, C.M. Julien, F. Gendron, Mater. Sci. Eng. B129 (2006) 232.

[12] N. Ravet, C. Michot, G. Nuspl, G. Liang, M. Gauthier, 210th ECS Meeting, Cancun, Mexico, 2006.
[13] A. Mauger, A. Ait-Salah, M. Massot, F. Gendron, K. Zaghib, C.M. Julien, ECS Trans. 3–36 (2007) 57–70.
[14] K. Zaghib, N. Ravet, A. Mauger, M. Gauthier, J.B. Goodenough, C.M. Julien, ECS Trans. 3–27 (2007) 119–129.
[15] J.F. Martin, A. Yamada, G. Kobayashi, S.-I. Nishimura, R. Kanno, D. Guyomard, N. Dupre, Electrochem. Solid State Lett. 11 (2008) A12.
[16] K. Zaghib, M. Dontigny, P. Charest, J.F. Labrecque, A. Guerfi, M. Kopec, A. Mauger, F. Gendron, C.M. Julien, J. Power Sources 185 (2008) 698.
[17] H.P. Klug, L.E. Alexander, X-Ray Diffraction Procedures for Polycrystalline and Amorphous Materials, Wiley, New York, 1974.
[18] C. Hammond, The Basic of Crystallography and Diffraction, Oxford University Press, New York, 1997.
[19] N. Amdouni, F. Gendron, A. Mauger, H. Zarrouk, C.M. Julien, Mater. Sci. Eng. B 129 (2006) 64.
[20] A. Ait Salah, A. Mauger, K. Zaghib, J.B. Goodenough, N. Ravet, M. Gauthier, F. Gendron, C.M. Julien, J. Electrochem. Soc. 153 (2006) A1692.
[21] M.T. Paques-Ledent, P. Tarte, Spectrochim. Acta A30 (1974) 673.
[22] C.M. Burma, R.J. Frech, Electrochem. Soc. 151 (2004) 1032.
[23] A. Ait-Salah, J. Dodd, A. Mauger, R. Yazami, F. Gendron, C.M. Julien, Z. Anorg. Allg. Chem. 632 (2006) 1598.
[24] C.M. Julien, Solid State Ionics 136 (2000) 887.
[25] N. Ravet, M. Gauthier, K. Zaghib, A. Mauger, J.B. Goodenough, F. Gendron, C.M. Julien, Chem. Mater. 19 (2007) 2595.
[26] P. Jozwiak, J. Garbarczyk, A. Mauger, F. Gendron, C.M. Julien, J. Non-Cyst. Solids 354 (2008) 1915.
[27] P. Jozwiak, J. Garbarczyk, M. Wasiucionek, I. Gorzkowska, F. Gendron, A. Mauger, C.M. Julien, Solid State Ionics 179 (2008) 46.
[28] G. Li, Y. Kudo, K.Y. Liu, H. Azuma, M. Tohda, J. Electrochem. Soc. 149 (2002) A1414.
[29] P. Amornpitoksuk, D. Ravot, A. Mauger, J.C. Tedenac, J. Alloys Compds. 440 (2007) 295.
[30] M. Kopec, J.R. Dygas, F. Krok, A. Mauger, F. Gendron, C.M. Julien, J. Phys. Chem. Solids 69 (2008) 955.
[31] K. Zaghib, A. Mauger, J. Goodenough, F. Gendron, C.M. Julien, Chem. Mater. 19 (2007) 3740.
[32] R.P. Santoro, R.E. Newnham, Acta Crystallogr. 22 (1967) 344.
[33] W.L. Roberts, T.J. Campbell, G.R. Rapp, in: Van Nostrand Reinhold (Ed.), Encyclopedia of Minerals, 2nd ed., Chapman & Hall, New York, 1990.
[34] M. Ayadi, J. Ferré, A. Mauger, R. Triboulet, Phys. Rev. Lett 57 (1986) 1165.
[35] P. Amornpitoksuk, D. Ravot, A. Mauger, J.C. Tedenac, Phys. Rev. B 77 (2008) 144405.
[36] A. Ben Mahmoud, J. Von Bardeleben, J. Cantin, A. Mauger, E. Chikoidze, Y. Dumont, J. Appl. Phys. 101 (2007) 13902.
[37] K. Persson, G. Ceder, D. Morgan, Phys. Rev. B73 (2006) 115201.
[38] P. Vuillet, J.P. Sanchez, D. Braithwaite, M. Amanowics, B. Malaman, Phys. Rev. B63 (2001) 184403.
[39] H. Fjellvag, A. Kjekshus, T. Chattopadhyay, H.D. Hochheimer, W. Hönle, H.G. von Schnering, Physica B&C 139–140 (1986) 305.
[40] F. Aguado, F. Rodriguez, P. Nunez, Phys. Rev. B 76 (2007) 1.
[41] H.C. Choi, J. Shim, B.I. Min, Phys. Rev. B 74 (2007) 172103.
[42] D. Morgan, A. Van der Ven, G. Ceder, Electrochem. Solid State Lett. 7 (2004) A30.
[43] C. Delacourt, L. Laffont, R. Bouchet, C. Wurm, J.-B. Leriche, M. Morcrette, J.-M. Tarascon, C. Masquelier, J. Electrochem. Soc. 152 (2005) A913.
[44] K. Zaghib, A. Mauger, F. Gendron, M. Massot, C.M. Julien, Ionics 14 (2008) 371.
[45] C.V. Ramana, A. Mauger, F. Gendron, K. Zaghib, C.M. Julien, J. Power Sources 187 (2009) 555–564.